



ELSEVIER

Journal of Nuclear Materials 270 (1999) 65–73

**journal of
nuclear
materials**

Characterization of UO_2 irradiated in the BR-3 reactor ¹

Suresh K. Yagnik *, Albert J. Machiels, Rosa L. Yang

Nuclear Power Group, EPRI, 3412 Hillview Avenue, Palo Alto CA 94304 USA

Received 11 May 1998; accepted 9 October 1998

Abstract

In order to better understand the behavior of irradiated UO_2 , six fuel rods containing fuel pellets fabricated by wet and dry processes were irradiated under various power histories in the BR-3 PWR (Mol, Belgium). Subsequent to the irradiation, extensive hotcell measurements were performed on complete rods, whole pellets, pellet cross sections or thin slices, and pellet fragments. The results of these measurements collectively underscore several key characteristics of high burnup (37–65 GWd/t) fuel. Although a clear separation of burnup effects and fuel temperature history effects was not possible, the pellet microstructure evolution can be defined in terms of four distinct radial zones. Further, fission gas release increased with burnup but grain growth was not found to be an integral part of the release mechanism. The onset of accelerated Xe release, as indicated by radial profiles by EPMA, corresponded well to a sudden increase in intragranular pore density within a narrow radial zone. Acicular precipitates having apparent similarity to U_4O_9 phase were found in etched as well as fractured surfaces in high burnup specimens. However, the phase structure was not confirmed and the precipitates might have originated due to changes in the fuel chemistry rather than stoichiometry. Finally, extensive fuel-cladding interaction with the formation of U–Cs–Zr compounds was observed for burnup >40 GWd/t. © 1999 Elsevier Science B.V. All rights reserved.

1. Introduction

The irradiation of UO_2 in LWRs produces a variety of physical and chemical changes. The microstructural changes in the fuel pellet such as densification, gaseous and solid fission-product swelling, and fission-product redistribution and release have a direct impact on thermal conductance of the fuel rod. Dimensions of fuel pellet and fuel-cladding gap vary with irradiation due to pellet swelling and cladding creep. In addition, the fissions alter the chemistry inside the fuel rod: new compounds and phases form within the pellet, at the pellet surfaces and grain boundaries, and in the gap, which, in turn, could change the stoichiometry of UO_2 with burnup.

Many such characteristics of irradiated UO_2 have been reported in numerous [1] studies. Barner et al. [2,3]

have summarized the High Burnup Effects Program whose principal objective was to investigate fission gas release in LWR rods irradiated to 47 GWd/t. Recent Japanese work [4,5] has focused on UO_2 microstructure and fission gas bubble behavior over a range of burnups. Many studies have appeared on now well-known phenomena of thermal conductivity degradation with burnup [1,6–11] and formation of rim-region [1,12–15] at burnups above ~45 GWd/t.

The subject continues to be of intense interest and new results are being published at a steady rate, especially at higher burnups. However, systematic information on characterizations of UO_2 irradiated to high burnups under typical LWR conditions (power levels 17–35 kW/m and burnups >35 GWd/t) is still lacking. In this paper we report on hitherto unpublished work sponsored by the Nuclear Fuel Industry Research (NFIR) Group under Phase I (1982–86). Several key high burnup features in fuel samples irradiated to 37–65 GWd/t, including fission gas retention and release, radial plutonium redistribution, characterizations of fuel-cladding interaction layer, and possible formation of U_4O_9 phase at high burnups are reported and discussed.

* Corresponding author. Tel.: +1-650 855 2971; fax: +1-650 855 1026; e-mail: syagnik@epri.com

¹ Work sponsored by NFIR Group under Phase I (1982–86).

2. Experimental

Six fuel rods encompassing two fuel fabrication routes were irradiated in the BR-3 PWR (Mol, Belgium). Five of these six rods (A1–A5) contained pellets fabricated by the wet process and the sixth rod (B1) contained the dry process pellets. Main as-fabricated characteristics of these fuel types are given in Table 1.

The fuel rods were of standard BR-3 dimensions (1136 mm total length, 1000 mm UO₂ stack length, 9.50 mm nominal diameter) containing standard dished geometry pellets with L/D ratio ~1.5. Initial U²³⁵ enrichment for the pellets was 8.25 wt% for rods A1 and A2, 5.76 wt% for rods A3–A5, and 4.95 wt% for rod B1.

The irradiation conditions are summarized in Table 2. The six fuel rods can be divided into three groups according to the fuel management strategy and the linear heat rating (LHR). Schematic plots of Power (LHR) vs. Cycle # for each of the three groups are also given in Table 2. The first group consisting of rods A1, A2 and A3 had similar power history during the first irradiation cycle. Rods A2 and A3 were irradiated for one and two additional cycles, respectively, to accrue additional burnup. Rod A4 was unique in that it was irradiated at a lower LHR in the first cycle than in the second cycle to assess the power history effects. Finally, rods A5 and B1 had a decreasing power rating during the two-cycle irradiation, with rod A5 operating at considerably higher power levels, as reflected by the final peak burnup values.

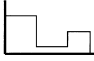
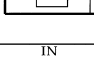
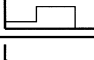
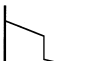

Subsequent to the irradiation, several sets of measurements were performed on:

1. complete rods (dimensional measurements, gamma spectrometry, and fission gas release by rod puncturing);
2. whole pellets (retained fission gas, radiochemical burnup, and density);
3. pellet cross sections or thin slices (radial microstructure evolution, pore density, and fission product distribution);
4. pellet fragments (scanning and transmission microscopy and phase structures).

Three fuel specimens per rod were selected to perform the destructive examinations of categories (2), (3), and (4) above. These were located at approximately 100% (index 1), 80% (index 2), and 60% (index 3) of the

Table 2

Irradiation conditions of the test rods in BR-3

Rod	1-cycle	2-cycle	3-cycle	Peak Burnup (GWd/t)
A1	IN (386)*			39.4
A2	IN (368)	OUT (139)		51.0
A3	IN (384)	OUT (82)	IN (187)	64.1
A4	OUT (226)	IN (300)		55.0
A5	IN (434)	OUT (234)		50.6
B1	IN (365)	OUT (186)		37.9

*Peak pellet LHR (W/cm)

* Peak pellet LHR (W/cm).

maximum rod burnup derived from the Cs¹³⁷ activity axial profile.

A complete assessment of the results from these 18 samples provided data on irradiated fuel behavior under different operating parameters for each of the comparative criteria listed in Table 3. A full review is provided in the detailed program reports [16–18]. We summarize and discuss below the key program results.

3. Results and discussion

3.1. Fission gas release

The six rods were punctured individually and the volume of collected gas was measured in each case. The gas samples were analyzed by mass spectrometry. From these data, the fractional gas release was computed using the Xe + Kr yield value with an overall estimated accuracy of ±2%. Fig. 1 shows the fractional gas release as a function of rod average burnup, which was determined by chemical analyses of fuel sample and axial power shape factors for each rod. Fractional release from rods A1, A2, and A3 appear to be consistent with their high power levels during the first cycle. The low fission gas release in rod B1 may be partly due to the dry pellet fabrication process. However, more importantly, rod B1 had a lower pellet-cladding gap (165 μm, compared to

Table 1

As-fabricated characteristics of fuel

Fuel type	Average grain size (μm)	Total porosity (%)	Inter-/intra-granular porosity	Open porosity (%)	Thermal stability* (%TD)
A: wet process	13.5	4–5	70/30	0.07	0.4
B: dry process	7.5	3–4	67/33	0.10	1.0

*Density increase after 24 h resintering at 1700°C.

Table 3

Fuel specimens for destructive examinations and main criteria for comparative study of the results

Specimen	Fuel management	Burnup (GWd/tM)	Peak LHR (W/cm)
<i>Criterion: Effect of power history at a given burnup and fabrication process</i>			
(a) Burnup ~40 GWd/tM			
A11	In	39.4	386
A22	In-out	41.3	298
A33	In-out-in	39.1	234
(b) Burnup ~50 GWd/tM			
A21	In-out	51.0	368
A32	In-out-in	50.6	303
A51	In-out	50.6	434
<i>Criterion: Increasing burnup, similar LHR in the first cycle</i>			
(a)			
A11	In	39.4	386
A21	In-out	51.0	368
A31	In-out-in	64.1	384
(b)			
A22	In-out	41.3	298
A32	In-out-in	50.6	302
<i>Criterion: Effect of management strategy</i>			
(a)			
A41	Out-in	55.5	300
A32	In-out-in	50.6	303
(b)			
A41	Out-in	55.6	300
A21	Out-in	51.0	368
(c)			
A42	In-out	45.7	249
A52	Out-in	43.0	369
<i>Criterion: Effect of fuel design (similar irradiation condition)</i>			
B11	In-out	37.9	365
A52	In-out	43.0	369

200 μm for all A rods) and a higher prepressurization (30 bars, compared to 20 bars for all A rods). Detailed temperature calculations showed [16] that rod B1 experienced maximum fuel center temperatures of ~1500°C only briefly during early irradiation and the tempera-

tures remained relatively low during subsequent irradiation.

Fission gas release has a well known temperature feedback effect due to reduced gap conductance caused by the released gases. Comparatively higher gas releases

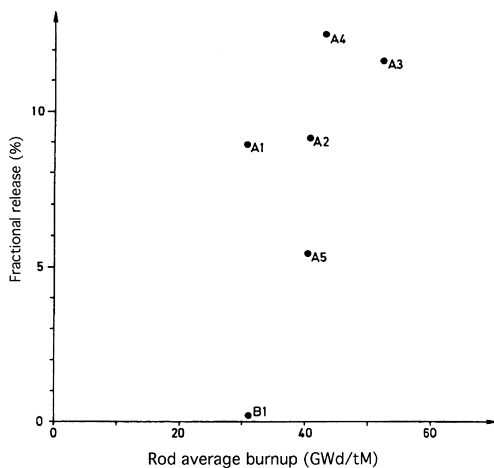


Fig. 1. Fractional release versus rod average burnup.

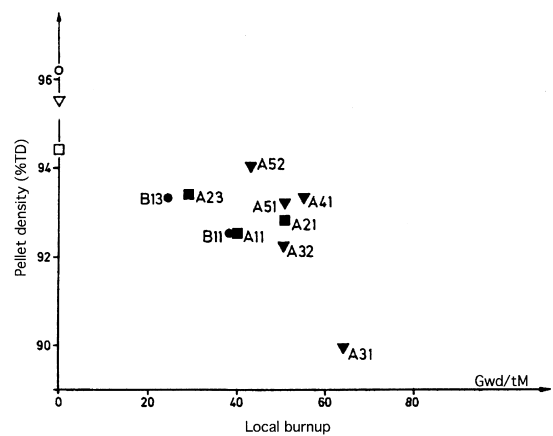


Fig. 2. Fuel specimen density as a function of burnup (open symbols indicate the unirradiated fuel densities).

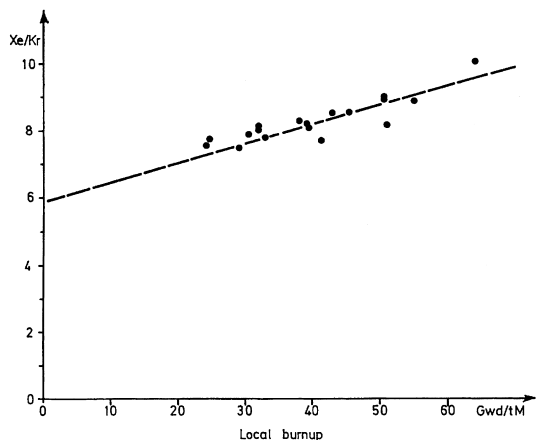


Fig. 3. Xe/Kr ratio versus local specimen burnup.

from rods A3 and A4 appear to be the result of their fuel management scheme (lower power operation in a given cycle followed by a higher power operation in the subsequent cycle). Presumably this operation strategy results in higher fuel temperatures in the later cycle due to the prior-cycle gas released to the gap and the resulting poorer gap conductance.

3.2. Pellet density and residual fission gas

The fuel density for 10 of the 18 samples of Table 3 was measured by the immersion technique. Large fuel fragments ($\sim 3\text{--}4$ g) were used for this purpose. The immersion liquid was monobromobenzene. The measurements are reported in Fig. 2 as %TD (theoretical density) based on a value of 10.96 g/cm³ for pure UO₂. The immersion densities were $93\% \pm 1\%$ TD for most samples, with the exception of the highest burnup sample A31 which was $\sim 90\%$ TD. Fuel densities inferred from optical measurements were significantly lower than those by immersion method.

Residual fission gas was analyzed in all 18 samples of Table 3. The irradiated pellet samples were dissolved in 10 M nitric acid. The quantity of evolved gases was measured and gas samples collected and purified by suitable cold traps were subsequently analyzed by mass spectrometry to determine residual Xe/Kr ratios in each case. This ratio increased with local burnup (Fig. 3) due to the progressively increasing contribution of fissions from Pu isotopes, which have lower yields for Krypton. Based on the three samples per rod analyzed for retained gas, a rod average value was calculated and compared with the rod average gas release data from rod puncturing. This provided a consistent mass balance based on cumulative yields of Xe and Kr.

As shown in Fig. 4, retained fission gas (%) decreases with local burnup and local power for all rods, except

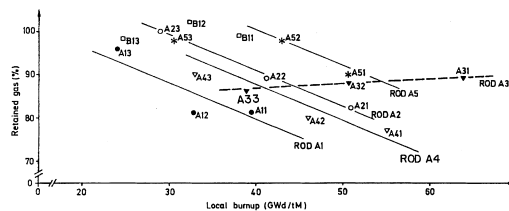


Fig. 4. Retained gas (%) versus local burnup.

for rod A3 where retained gas values do not show a decreasing trend. This can be due to the unique power history of rod A3: first, A3 had the highest fuel duty in that it was operated for all 3 cycles. Second, detailed temperature calculations indicate [16] that even the low power zone (e.g., sample A33) experienced a maximum fuel center temperature of 1250°C , a temperature well above the fission gas release threshold temperature [19] expected for the three A3 samples.

3.3. Plutonium redistribution

Buildup of plutonium in the fuel increases with irradiation time; however, the rate of increase becomes progressively slower with burnup as plutonium begins to be consumed by fissioning. Average plutonium content in fuel samples, determined by radiochemical method, gave an average buildup rate of $0.1\%/10$ GWd/t. By taking micro-drill samples from various radial locations across a fuel disc, an average buildup rate of nearly five times as high was measured for the pellet periphery. Radial profiles of Pu measured by EPMA also confirmed the sharp increase in plutonium contents at the periphery. The plutonium concentration rapidly decreased over the first 30 μm from the pellet surface, and remained relatively flat in the interior. Detailed EPMA profiles, documented in Ref. [16], are believed to be the earliest systematic documentation of the kind. EPMA profiles and microstructural evolution, especially of the so called fuel rim-region, have since been extensively reported [1,12–15] since the mid 1980s.

3.4. Fuel-cladding interaction layer

The extent of fuel-cladding interaction, as observed by cross-sectional macrographs, varied circumferentially and with burnup. As much as $25\text{--}65\%$ of the circumferential surface area of high burnup samples (A21, A31, A32, A41, and A51) showed the presence of an interaction layer and, in addition, an inner zirconium oxide layers $\approx 8\text{--}10$ μm thick. A strong fuel-cladding bonding was indicated in these samples by (i) pieces of fuel adhering to the cladding inner surface or (ii) cladding inner oxide sloughing off from the cladding inner surface. In contrast, the low burnup sam-

ples A23 and B13 had neither the interaction layer, nor any significant zirconium oxide layer, except for a few patches of spongy deposits. In all samples examined, a prerequisite of ZrO_2 formation appeared to be a strong solid-solid contact between fuel and cladding. It was, therefore, concluded that zirconium oxide on the cladding inner surface was not formed via direct vapor phase transport of oxygen from fuel to cladding, but rather via the oxygen bearing U–Cs–Zr compounds that acted as intermediary oxygen transport agents.

Fig. 5(a) shows a typical reaction zone from sample A31. At peak power of 384 W/cm, this sample experienced a strong PCMI and extensive fuel cracking. Adjacent to the thin light gray ZrO_2 layer on the cladding inner, is a dark gray phase, which is predominantly rich in Zr and Cs. This is followed by a highly porous U + Cs compound that is often associated with fuel cracks. This porous phase is apparently viscous at operating temperatures as it appears to have flowed into these fuel cracks. The picture that emerged from a number of X-ray maps and X-ray line scans of the region corresponding to Fig. 5(a) is schematically sketched in Fig. 5(b). Other high burnup samples were also qualitatively similar.

3.5. Fuel microstructure evolution

The fuel microstructure evolution with burnup can be explained in terms of four distinct radial zones, as shown in Fig. 6. Although some differences in the onset and degree of restructuring were observed among various samples, the four zones were qualitatively quite similar in all. TEM observation indicated the presence of very small bubbles (~ 2 nm diameter) throughout the fuel cross-section. The four zones of Fig. 6 differ mainly in terms of large sub-micro meter and micro meter size pores and bubbles. These zones are discussed below with the aid of Fig. 7 which shows the radial pore distribution determined by image analysis.

Zone I (fuel periphery): This zone appears at pellet average burnup of about 35 GWd/t and is fully defined by 50 GWd/t. The radial extent of this zone corresponded with the Pu enrichment at the periphery which was described in a previous section. The zone showed high intragranular porosity and sub division of grains with ragged grain faces observable under high resolution SEM. As seen in Fig. 8, Xe depletion at pellet periphery was not observed, despite corresponding grain subdivision. This could be due to relatively lower burnup of the samples examined compared to the threshold burnup for

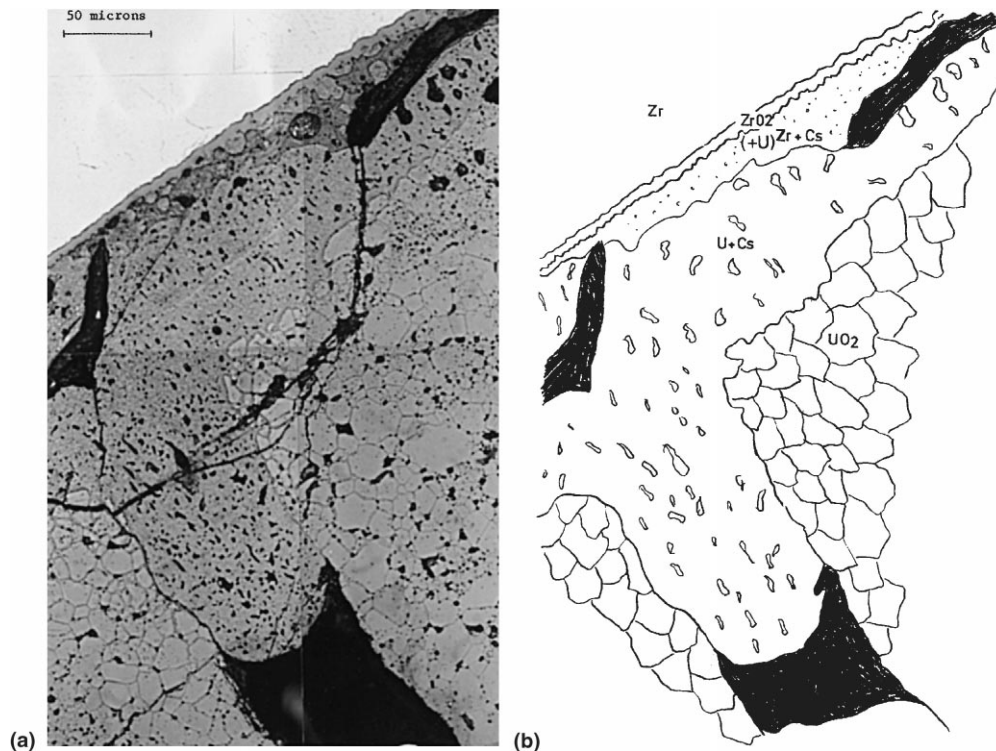


Fig. 5. (a) Fuel microstructure of the fuel-cladding reaction zone in specimen A31. (b) Identification of elements by X-ray mapping in the fuel-cladding interaction zone of Fig. 5(a).

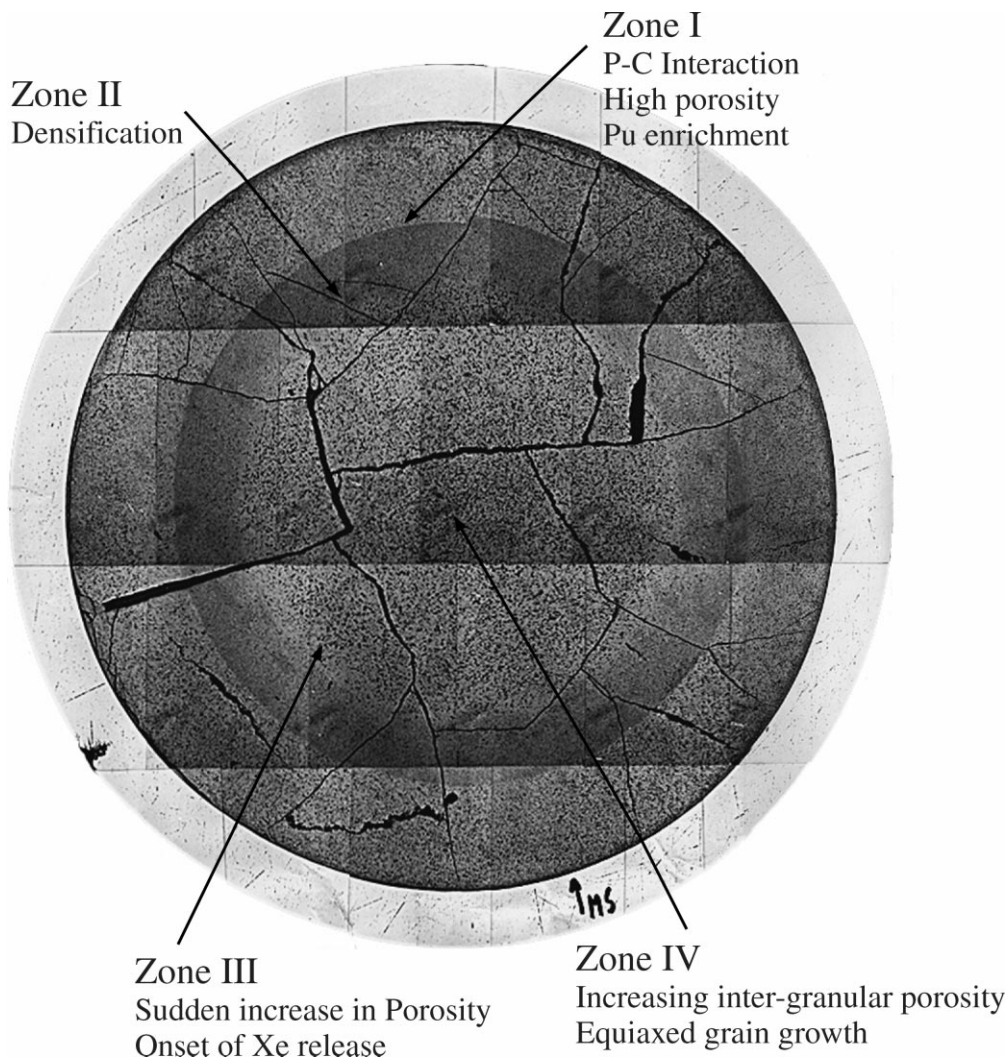


Fig. 6. Photomicrograph montage of the cross-section of specimen A31 illustrating the four restructured zones.

Xe depletion, since believed to be in the range of 65–75 GWd/t [24].

Zone II (densified fuel): The high porosity of Zone I is reduced dramatically within a radial distance of a few hundred micro meter (Fig. 7), reaching a minimum around 2–3%. This zone of low porosity is Zone II where fuel densification is observed. SEM comparisons of as-fabricated and as-irradiated samples confirmed fuel densification in this zone due to elimination of sub-micro meter size pores.

Zone III (transition porosity): Further inwards from Zone II, a sudden transition to high porosity is observed in the outer parts ($r > 0.5$) of the pellet cross-section. This transition in microstructure between Zones II and III is quite sharp. It occurs within a few grain-widths, as seen in the optical microscopy of chemically-etched

samples. The entire Zone III (and the associated local high porosity region) is about 2–3 mm wide. The pore density distribution shown in Fig. 7 also attests to the sharp transition from Zone II to III. The Xe profile by EPMA (Fig. 8) for a nominally identical sample to that of Fig. 7 also shows a sharp decrease in Xe concentration at approximately at the same radial location. This confirms that the sudden increase in the intragranular pore density within a narrow radial zone is directly related to Xe release from this zone.

Zone IV (fuel center): In the central parts of the fuel the porosity becomes comparable to that of Zone II. The pores coalesce into large intergranular bubbles. The transition to this Zone from Zone III is gradual in comparison to the Zone II to III transition described above. This is characterized by gradual loss of intra-

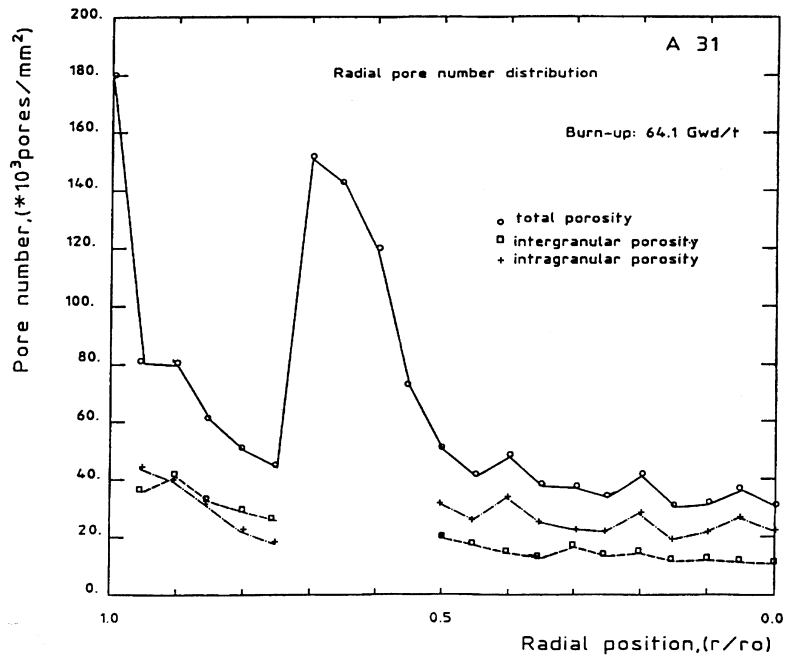


Fig. 7. Radial pore number distribution.

granular pores and increase of intergranular pores as pellet center is approached from Zone III.

3.6. Formation of U_4O_9

Formation of U_4O_9 may be expected if the fuel becomes hyperstoichiometric with burnup. Acicular precipitates were observed in all irradiated fuel samples on chemically etched surfaces examined by optical microscopy and SEM as well as on fractured surfaces observed by SEM. Examples of these are shown in Figs. 9 and 10. These precipitates were more readily observable at the outer radial positions ($r > 0.7$) of the samples. The phase structure of these precipitates was not determined,

but their morphology and relative orientation appear to be similar to those reported by Schaner [20] in his study of the UO_2 – U_4O_9 phase diagram.

To assist in identifying this precipitate phase, archive pellets of Type A and B fuel were oxidized to UO_{2+x} and examined by electron microscopy. This investigation confirmed that needle-shaped U_4O_9 phase does indeed appear on chemically-etched surfaces but not on the fracture surfaces in SEM.

Although the possibility of making fuel hyperstoichiometric by fission is commonly invoked, the present study could not confirm that the acicular precipitates in the irradiated samples (Fig. 9) were indeed in U_4O_9 phase. These precipitates may have originated due to changes in the fuel chemistry rather than hyperstoichiometry [21]. More recently, Davies et al. [22] have concluded that such acicular features are defects or intragranular microcracks. Similarly Matzke [23] has reported direct oxygen potential measurements and concluded that high burnup fuel is not hyperstoichiometric.

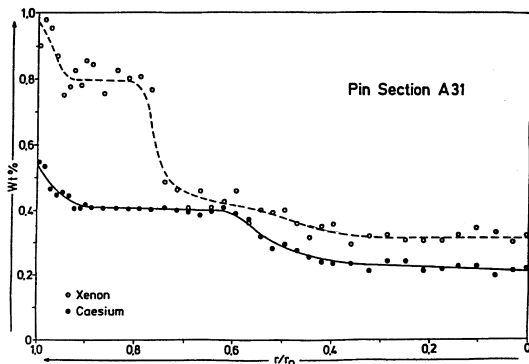
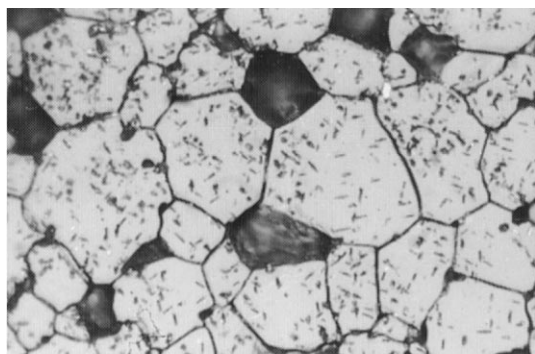


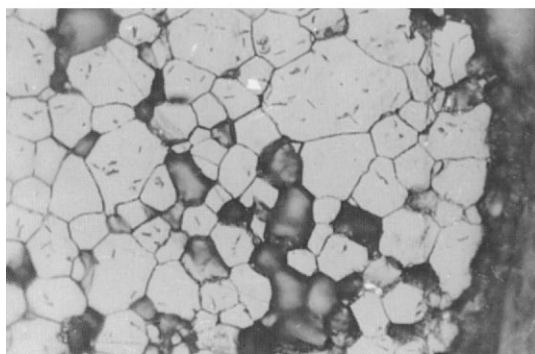
Fig. 8. Xenon and cesium radial distribution in specimen A31.

4. Conclusions

Some of the myriad changes which occur in UO_2 irradiated to high burnup were described. Prominent among them is the microstructural evolution which can be defined in terms of four distinct radial zones. The onset of accelerated Xe release, as indicated by radial



(a) A33



(b) B11

Fig. 9. Acicular phase precipitates at pellet outer rim in chemically etched specimens (a) A33 and (b) B11.

profiles by EPMA, corresponds well to a sudden increase in intragranular pore density within a narrow radial zone. Fission gas release increases with burnup (and the retained gas decreases), but grain growth was not found to be an integral part of the release mechanism. An extensive fuel-cladding interaction with the formation of U–Cs–Zr compounds is observed for burnup >40 GWd/t.

Acicular precipitates having apparent similarity to U_4O_9 phase were found in etched as well as fractured surfaces in high burnup specimens. However, the phase structure was not confirmed, and precipitates might have originated due to changes in the fuel chemistry rather than stoichiometry.

Acknowledgements

This work was sponsored by the EPRI-managed NFIR Group and led by Belgonuclaire, SA (Belgium) with technical collaborations from CEN/SEK (Bel-

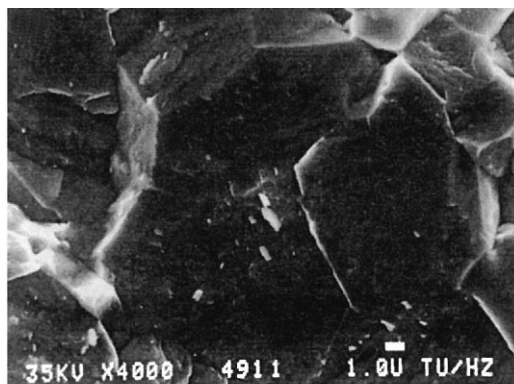
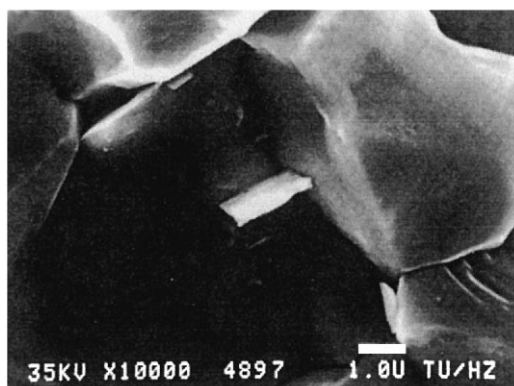
(a) $r/r_0 = 0.45$, $\times 4000$ (b) $r/r_0 = 0.65$, $\times 10,000$

Fig. 10. SEM observation of platelet-shaped intragranular precipitates in specimen A52 at two radial locations.

gium), TUI (Germany), and then CEGB (UK). The authors are thankful to the members of the NFIR Steering Committee for their technical guidance and the permission to publish the work.

References

- [1] See papers on the subject, in: Proc. Internat. Topical Meetings on LWR Fuel Performance at Avignon, April 1991, West Palm Beach, April 1994, and Portland, March 1997.
- [2] J. Barner et al., Nucl. Technol. 102 (1993) 210.
- [3] J. Barner et al., J. Nucl. Mater. 188 (1992) 19.
- [4] S. Kashibe et al., J. Nucl. Mater. 206 (1993) 22.
- [5] K. Ume et al., J. Nucl. Mater. 188 (1992) 65.
- [6] R. Brandt, G. Neuer, J. Non-Equilib. Thermodyn. 1 (1976) 3.
- [7] R. Brandt, G. Neuer, A critical review on the subject translated by Center for Information and Numerical Data,

- Analysis and Synthesis (CINDAS), Purdue University, April 1976.
- [8] E. Kolstad, C. Vitanza, *J. Nucl. Mater.* 188 (1992) 104.
- [9] K. Yamamoto et al., *J. Nucl. Mater.* 204 (1993) 85.
- [10] C. Bagger et al., *J. Nucl. Mater.* 211 (1994) 11.
- [11] P. Lucuta et al., *J. Nucl. Mater.* 217 (1994) 279.
- [12] S. Pati et al., Proc. Intl. Topical Meeting on LWR Fuel Performance, Williamsburg, April 1988, p. 204.
- [13] Hj. Matzke et al., *J. Nucl. Mater.* 166 (1989) 165.
- [14] Hj. Matzke, *J. Nucl. Mater.* 189 (1992) 141–148.
- [15] T. Kameyama et al., *Nucl. Technol.* 106 (1994) 334.
- [16] Properties of UO₂ Irradiated to high burnups, Final Report on EPRI Project X101-5, NP-5191-LD, April, 1987, prepared by Belgonucleaire SA.
- [17] Properties of UO₂ Irradiated to high burnups, Topical Report on EPRI Projects X101-5 and X101-7, NP-5189-LD, April 1987, prepared by Belgonucleaire, SA (Belgium) and Central Electricity Generating Board, UK.
- [18] Properties of UO₂ Irradiated to high burnups (TEM and SEM Study), Final Report on EPRI Project X101-7, NP-5188-LD April, 1987, prepared by Central Electricity Generating Board, UK.
- [19] E. Kolstad et al., High Burnup Fuel Behavior Studies by In-pile Measurements, Proc. Intl. Topical Meetings on LWR Fuel Performance at Avignon, vol. 2, 1991, pp. 838–849.
- [20] B. Schaner, *J. Nucl. Mater.* 2 (1960) 110.
- [21] M. Magnanelli, P. Potter, *J. Nucl. Mater.* 114 (1983) 168.
- [22] J.H. Davies et al., Behavior of high O/U fuel, paper presented at the Enlarged HPG Meeting, Bolkesjo, Norway, 1994.
- [23] Hj. Matzke, *J. Nucl. Mater.* 223 (1995) 1.
- [24] J. Spino et al., *J. Nucl. Mater.* 256 (1998) 189.